The Dynamic Response of the Winter Stratosphere to an Equable Climate Surface Temperature Gradient

Robert L. Korty* and Kerry A. Emanuel

Program in Atmospheres, Oceans, and Climate, Massachusetts Institute of Technology, Cambridge, Massachusetts

ABSTRACT

This work investigates the dynamic and thermal response of the winter stratosphere to the presence of a weak meridional surface temperature gradient. Previous work suggested that polar stratospheric clouds could have played a decisive role in maintaining high-latitude warmth, especially over continental interiors, during the polar nights of the late Paleocene and early Eocene epochs; both a chemical source of additional water vapor and a dynamical feedback between the surface climate and stratospheric temperatures have been proposed as mechanisms by which such clouds could form. A principal goal of this work is to investigate the latter problem using a general circulation model with stratospheric resolution that is forced with a very weak surface temperature gradient. It is found that temperatures in the lower stratosphere do not deviate significantly from the control run, which results from a robust flux of wave activity into the winter stratosphere. The strength of the stratosphere's residual circulation increases slightly in the presence of the weak gradient, as wavenumber 3 begins to propagate to stratospheric altitudes. Changes in the zonal wind field that allow for the altered propagation are in balance with a weakened temperature gradient through the full depth of the troposphere. These simulations also suggest that the tropospheric thermal stratification could be maintained by moist convection at all latitudes in warm climate states with a weak temperature gradient.

1. Introduction

There is ample evidence from fossils and geochemical proxies that polar temperatures throughout much of the Phanerozoic eon were mild, particularly during the Paleocene and Eocene epochs of the early Cenozoic era[1] (e.g., Sluijs et al. 2006; Huber et al. 2000). Contemporaneous tropical temperatures were likely warmer than today (Pearson et al. 2001), but the departures from current values were smaller than at high latitudes. Taken together, there is persuasive evidence that a much weaker equator-to-pole temperature gradient existed during these warm climates than is present today; this climate state has proved puzzling for dynamicists, given that the growth rate of the atmospheric eddies principally responsible for transporting heat poleward would weaken in the presence of such a gradient (Lindzen and Farrell 1980). High loads of carbon dioxide (Barron and Washington 1985), strong ocean heat transport (Barron 1983; Emanuel 2002; Korty et al. 2007), and polar stratospheric clouds (Sloan et al. 1992; Sloan and Pollard 1998; Kirk-Davidoff et al. 2002) have all been discussed as components of the warm climate problem.

Sloan et al. (1992) first proposed that increased concentrations of methane from large wetlands during the early Cenozoic would provide a source for stratospheric water vapor, allowing optically thick clouds to form in the polar vortex. Subsequent tests showed that, if these clouds were ubiquitous and thick enough, their impact on the surface climate of high latitudes could be substantial (Sloan and Pollard 1998; Sloan et al. 1999; Peters and Sloan 2001). Work by Dickens et al. (1997) and

---

[1] The Phanerozoic eon spans the most recent 540 million years of the earth's history; the Cenozoic era began 65 million years ago (Mya), and the Paleocene (65–56 Mya) and Eocene (56–34 Mya) were the first two epochs of this era.

---

* Current affiliation: Department of Atmospheric Sciences, Texas A&M University, College Station, Texas.

Corresponding author address: Robert L. Korty, Department of Atmospheric Sciences, Texas A&M University, 3150 TAMU, College Station, TX 77843-3150.
E-mail: korty@alum.mit.edu

Bralower et al. (1997) suggested that methane levels may have been further elevated at the Late Paleocene Thermal Maximum (LPTM) (56 Mya) from a sudden release of methane clathrates.

Kirk-Davidoff et al. (2002) proposed a separate, dynamic feedback between the surface meridional temperature gradient and polar stratospheric clouds, which, if operable, would create conditions favorable for polar stratospheric clouds whenever the surface temperature gradient is weak. Their hypothesis is that the weaker surface gradient would diminish tropospheric wave activity and reduce the upward flux of wave activity into the stratosphere that drives the Brewer–Dobson circulation and warms the polar vortex. One implication of their hypothesis is that, for any climate in the past or future in which the surface temperature gradient weakens, there could be a notable response in the winter stratosphere.

But the details of how the stratospheric circulation and temperatures should change in the presence of a weak gradient are not clear, and previous work suggests the response might not be simple. Rind et al. (1990, 1998) investigated the response of the middle atmosphere to a doubling of carbon dioxide and a concomitant weakening of the surface temperature gradient. Using a version of the Goddard Institute of Space Studies (GISS) global climate model extended through middle atmosphere levels (Rind et al. 1988a,b), they found that the overturning circulation increased in the warmer climate with elevated carbon dioxide. While tropospheric eddy energy decreased in those experiments, energy in the longest planetary-scale waves increased; they attributed this increase to the differing radiative impacts that higher carbon dioxide loads have on low and high altitudes. But in a full study of the Paleocene, which included a weaker temperature gradient, altered and reduced topography, and doubled carbon dioxide, they found a weaker stratospheric circulation (Rind et al. 2001).

Additionally, as Kirk-Davidoff et al. (2002) note, a clear link between the surface temperature gradient and deposition of angular momentum in the stratosphere is not obvious, as weaker jets, in thermal wind balance with the reduced gradient, might allow a broader spectral range of planetary waves to vertically propagate (Charney and Drazin 1961). Given the role that eddies play in maintaining tropospheric stability in the extratropics in the present climate (Stone 1978; Schneider 2004, 2007), it is not clear a priori what a very weak, imposed surface temperature gradient will mean for higher altitude temperature gradients and jet speeds when eddy activity is reduced.

There have been many previous efforts to model specific warm periods; numerous studies focused on the late Paleocene and early Eocene epochs, which are the most recent examples of equable climate surface conditions. Studies by O'Connell et al. (1996), Huber and Sloan (1999, 2000), and Sloan et al. (2001) imposed various configurations of weak sea surface temperature (SST) gradients and investigated the atmospheric and land surface responses. Our work differs from these earlier studies in that we explicitly resolve the stratosphere in order to investigate the dynamic response to a weak surface temperature gradient. Rind et al. (2001) applied a middle atmosphere model to examine the stratospheric response to Paleocene epoch conditions, but their study included comprehensive changes to the surface forcing that are specific to that time period.

To understand how the stratosphere relates to the surface climate across a variety of time scales in which carbon dioxide, topography, and the surface temperature gradient have all varied, it is important to examine how the stratosphere responds to changes in each of these forcings. Is the dynamic and thermal state of the winter stratosphere a function of the surface temperature gradient, particularly in climate states far removed from the present one? In this paper, we study the response to a very weak surface temperature gradient alone; to investigate this question we use the National Center for Atmospheric Research's (NCAR) Community Atmosphere Model version 3 (CAM3) but modified by extending vertical resolution into the mesosphere.

2. The Community Atmosphere Model

The standard version of CAM3 has 26 vertical levels, which extend to an altitude around 3 hPa (approximately 40 km) (Collins et al. 2006). To separate the model top from the stratosphere, which is the principal region of interest in the experiments presented here, the vertical resolution above 100 hPa has been increased and the model top has been moved into the middle mesosphere, around 63 km; the new version contains 40 vertical levels. Additionally, Rayleigh friction has been added to the levels above 3 hPa to dampen waves radiating out of the stratosphere. This reduces the reflection of these waves off of the model top and gives the energy passing across the stratopause a sink at high altitudes. These changes closely follow the techniques of Boville (1986).

The Rayleigh friction term added to the zonal momentum equation provides a crude parameterization of the effect of breaking gravity waves in the mesosphere in addition to reducing the reflection of waves off of the

top boundary. The frictional damping coefficient is determined by

$$K_R = \frac{2}{3}\left[1 + \tanh\left(\frac{z - 63}{H}\right)\right]\text{day}^{-1}, \qquad (1)$$

where z is the height in kilometers and H is the scale height (7.5 km). This form is identical to that used in Boville (1986), except that the amplitude has been increased by a factor of 2 in order to more accurately represent jet speeds near the stratopause in simulations of the present climate (B. Boville 2004, personal communication). Boville (1986) notes that the Rayleigh friction term should not be regarded as an accurate representation of mesospheric dynamics, which the model does not explicitly resolve. The magnitude of K_R that Boville (1986) used was chosen to match the damping estimated from observations by Smith and Lyjak (1985) in the mesosphere and to be insignificant in the stratosphere. The addition of this friction damps the jet toward zero over time scales of a few days in the lower mesosphere; below 40 km, the damping is negligible.

For all runs presented here, we used the Eulerian spectral dynamical core with triangular spectral truncation at 31 wavenumbers (T31). We made no other changes to the model code, and the reader is referred to Collins et al. (2006) for additional detail. The focus of this paper will be on a comparison of three separate experiments: a control experiment designed to replicate the present climate and two others forced with a weak surface temperature gradient.

As our present focus is on the response to changes in the surface temperature gradient alone, the runs were forced with current geography and an imposed monthly varying sea surface temperature field. Continental surface temperatures are explicitly calculated by the Community Land Model (CLM3), which is coupled to CAM3 (Dickinson et al. 2006). The control run was forced using contemporary SST data;[2] in the discussion that follows, this simulation is called "Present," as it models the current atmosphere. The simulations of warm climates were forced with an idealized, zonally symmetric sea surface temperature profile.[3] For these runs, sea surface temperatures were

---

[2] We used the standard file for stand-alone integrations of CAM3. As discussed in Collins et al. (2006), this SST dataset is a blended product combining the global Hadley Centre Sea Ice and SST (HadISST) dataset (Rayner et al. 2003) and the Reynolds et al. (2002) dataset.

[3] For comparison, we forced a second simulation of the current climate with a zonally averaged version of the contemporary dataset; qualitatively, there were no differences in the stratosphere between this run and Present.

$$T(\varphi, t) = \Delta T \cos\left[\frac{\pi}{2}\sin\left(\frac{\pi[\varphi - \varphi_m(t)]}{180°}\right)\right] + (T_m - \Delta T),$$
$$(2)$$

where φ is the latitude in degrees, t is day of the year, ΔT is the equator-to-pole temperature difference; $\varphi_m(t)$ is the latitude at which the warmest sea surface temperature, T_m, can be found on day t. The latitude at which T_m resides oscillates on an annual cycle:

$$\varphi_m(t) = \frac{(\varphi_n - \varphi_s)}{2}\cos\left(2\pi\frac{[t - t_n]}{365}\right) + \frac{(\varphi_n + \varphi_s)}{2}. \quad (3)$$

Here φ_n (φ_s) is the northern- (southern)most latitude at which T_m occurs, and t_n is the day on which T_m reaches φ_n. By setting t_n to be noon on 1 August (day 213.5), the warmest sea surface temperatures will settle near φ_n during the Northern Hemisphere summer before migrating south toward φ_s, reaching it six months later. Choosing φ_n to be 8°N, φ_s to be 2°S, T_m to be 30°C, and ΔT to be 10°C, Eqs. (2) and (3) produce an idealized, warm profile over the entire planet. There is no sea ice in the warm simulations as the ocean temperatures are always too warm for it to form; in the simulation of the present climate, monthly varying sea ice is prescribed with the default dataset. These choices for φ_n and φ_s closely mimic the present range of T_m (e.g., Lindzen 1990). There is no reason to expect these to remain fixed through geological time, but the small value of ΔT strongly limits the variability of temperatures in both space and time. Temperatures in the Tropics are confined to 28°–30°C, while high-latitude ocean temperatures are never colder than 20°C year-round.

A comparison between the contemporary gradient used in Present and the one used for our two warm climate experiments is shown in Fig. 1. The figure shows the annually and zonally averaged SSTs from the standard version of the model (Present) and the one imposed in our two warm climate simulations ["weak temperature gradient" (WTG) and "radiation" (RAD)], which was calculated by Eqs. (2) and (3); the interannual variability of the zonally averaged SSTs are shaded around both curves. For the warm climate simulations, the low pole-to-equator temperature difference confines temperatures at each model point to vary little over the course of the year. This temperature profile produces a meridional gradient that is more gradual than that supported by proxy data, but we favor it for several reasons. First, the most striking qualitative features of warm climates are captured: tropical temperatures are only slightly warmer than the values observed today, while high-latitude temperatures are kept mild enough to inhibit sea ice. The choice of 10°C for ΔT
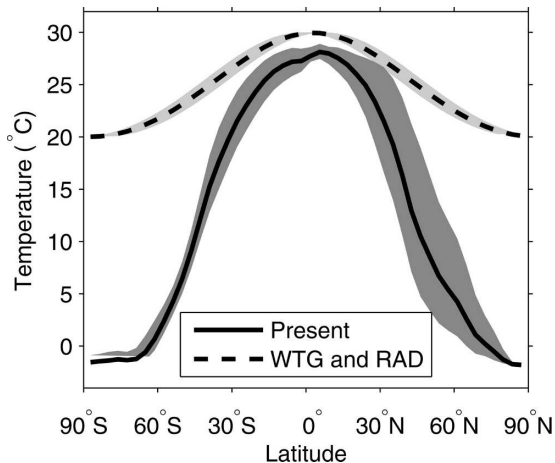
FIG. 1. Zonal- and annual-mean SSTs prescribed in the simulations. The gray bands show the temporal range of the zonal mean SST.

produces a SST gradient that is quite weak, and the temperature gradient has likely been stronger than this throughout the Cenozoic era.[4] Our point is not to simulate conditions from the Eocene or any other time period directly. This study focuses on mechanisms, and we therefore choose a very weak temperature gradient in order to test the limits of the proposed dynamic feedback. If a temperature gradient this weak does not force the stratosphere to a colder state conducive to large-scale polar stratospheric cloud formation, a dynamic response to the surface temperature gradient alone is unlikely to have led it to such a state at any point when a more moderate gradient existed.

We present two simulations using the same weak temperature gradient, but they differ in the concentrations of key longwave absorbers. One experiment retains the present concentrations of carbon dioxide (355 ppm) and methane (1.714 ppm) while using the weak surface temperature gradient specified by Eqs. (2) and (3); we call this simulation "Weak Temperature Gradient." The second warm climate experiment elevates carbon dioxide to 1500 ppm and methane to 10 ppm while using the weak temperature gradient shown in Fig. 1, and we refer to it as "Radiation." No other changes were made: the topography and location of the

continents is constant and ozone concentrations are specified for the present climate.[5] Our presentation will focus on the contrast between WTG and RAD and the control run, Present, to assess how changes in the surface temperature gradient affect the winter stratosphere. Because we impose SSTs, the model does not require many years of integration to reach a steady state. We integrated each of our experiments for 20 model years; the results presented in this paper are from averages over the last 5 years of data.[6]

3. Thermodynamic structure of the polar stratosphere

Given the limited concentrations of water vapor present in the polar stratosphere, clouds at these altitudes are restricted in size and thickness, particularly in the Arctic owing to milder mean temperatures. To see why large-scale clouds are not possible in the Arctic vortex in the present climate, consider the observational data in Fig. 2a. Zonal and time-mean temperatures from Rees et al. (1990) are plotted along the dotted curve.[7] These may drop to 200 K in the Arctic vortex in the middle stratosphere, but this is far warmer than the temperatures required for condensation of a parcel of air containing 5 ppmv, the ambient concentration of water in the polar stratosphere (e.g., Remsberg et al. 1984; Kent et al. 1986; MacKenzie et al. 1995) (The temperatures and pressures at which a parcel of air containing 5 ppmv of water vapor will be saturated are shaded in dark gray). Thus, clouds in the present stratosphere are confined to the smaller regions and times when temperatures fall to the frost point.[8] The frost point temperature T_f is the temperature at which ice saturation occurs:

$$e^{\#}(T_f) = e, \qquad (4)$$

[4] Recent estimates from the Arctic Ocean suggest high-latitude temperatures at the Late Paleocene Thermal Maximum may have been as high as 23°C, with values as warm as 18°C common during the Paleocene and Eocene epochs (Sluijs et al. 2006; Moran et al. 2006). Combined with tropical estimates from Pearson et al. (2001), these latest reconstructions would suggest the pole-to-equator temperature gradient was likely about 15°C during the early Cenozoic.

[5] We used the default ozone concentrations for CAM3; they vary with latitude, season, and altitude.

[6] Dickinson et al. (2006) analyzed output starting with the 11th year of an integration of CAM3 and CLM3 when climatological SSTs were imposed. We are interested in the mean climate state of each simulation and average over five years of data; a longer integration would be required for an examination of year-to-year variability.

[7] These data were compiled in 1986, and temperatures have decreased in the stratosphere over the past few decades. Thompson and Solomon (2005) found that Northern Hemisphere extratropical stratospheric temperatures have cooled at the rate of about 0.6 K decade^{-1} since 1979.

[8] The frost point serves as the threshold temperature for Type II clouds in the stratosphere, which are composed of ice crystals. Type I clouds, which are composed of a nitric acid–water compound, can form at temperatures about 3–4 K warmer than the frost point (e.g., Carslaw et al. 1994).
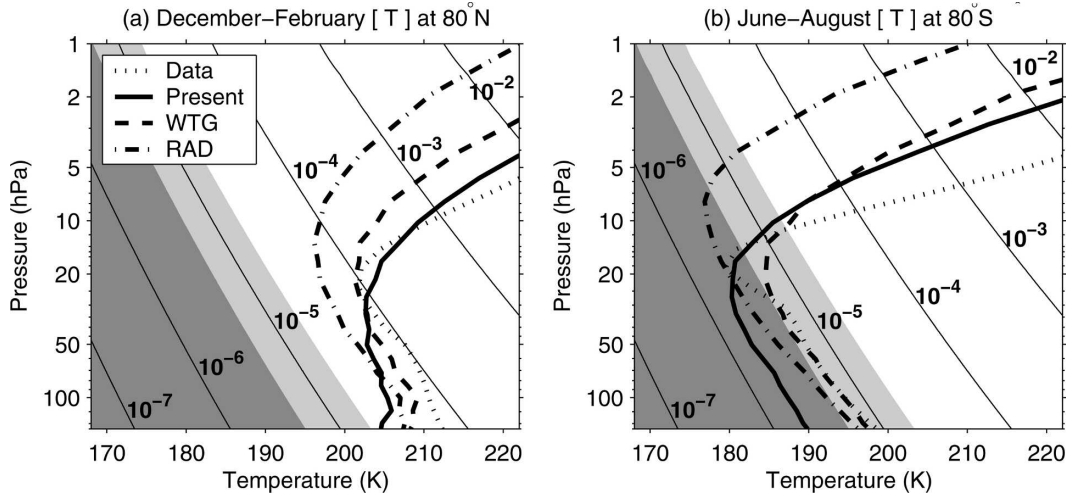
FIG. 2. Zonally and seasonally averaged T (a) at 80°N from observations (dotted) and from averages over the last five years of Present (solid), WTG (dashed), and RAD (dashed–dotted). Saturation vapor curves are plotted with thin black lines and are labeled with the maximum amount of vapor (parts by volume) a parcel at that T and p can hold. An air parcel containing 5-ppmv water vapor will be saturated at temperatures and pressures shaded in dark gray; a parcel containing 20 ppmv will be saturated also in areas shaded in light gray. (b) As in (a) but at 80°S during the Southern Hemisphere winter.

where e is the partial pressure of water (vapor pressure), and $e^{\#}$, the saturation vapor pressure over ice, is defined empirically (e.g., Emanuel 1994, p. 120):

$$\ln e^{\#} = 23.33086 - \frac{6111.72784}{T} + 0.15215 \ln T, \quad (5)$$

where the unit of T is in kelvin. The amount of water vapor a parcel of air can hold is additionally a function of pressure. The saturation specific humidity over ice $q^{\#}$ is defined (e.g., Emanuel 1994, p. 108)

$$q^{\#} = \frac{\rho_v^{\#}}{\rho_d + \rho_v^{\#}} = \frac{\epsilon e^{\#}}{p - e^{\#}(1 - \epsilon)}, \quad (6)$$

where ρ_v is the density of water vapor, ρ_d is the density of dry air, ϵ is the ratio of the molecular weight of water to the mean molecular weight of dry air (this is equivalently the ratio of the weighted mean gas constant for dry air to the gas constant of water vapor, $R_d/R_v \approx 0.622$), and the pound superscripts (#) denote saturation over ice. The saturation vapor curves from Eq. (6) are plotted in Fig. 2 and labeled with concentrations in parts by volume.[9]

Temperatures must cool 15–20 K, local water vapor

---

[9] The form of Eq. (6) gives values for $q^{\#}$ as a mass ratio. To convert to the parts by volume plotted in Fig. 2, one must multiply by the ratio of the weighted mean molecular mass of the parcel to the molecular mass of water vapor. At these low concentrations of water, the parcel is effectively dry, and the mean molecular mass of the parcel is very nearly the molecular mass of dry air.

concentrations must rise by a factor of 10 to 15, or some combination of both must occur in order for widespread polar stratospheric cloud formation to occur in the present Arctic. By contrast, temperatures in the Antarctic are substantially colder; Fig. 2b shows the zonal-mean temperatures for June–August at 80°S. These data (Rees et al. 1990) lie near the threshold for condensation of a parcel of air with 5 ppmv water vapor, and polar stratospheric clouds are far more common in the Antarctic winter than in the Northern Hemisphere. Still, observations from the field campaigns in the Antarctic show that reaching the local frost point of water on the synoptic scale does not guarantee that any clouds will be thick enough to affect the surface climate (e.g., Rosenfield 1992, 1993). But, if clouds were ubiquitous during warm climates, such as those tested by Sloan and Pollard (1998), a minimum thermodynamic requirement is that large-scale temperatures remain at or below the frost point for the duration of the polar night.

4. Stratospheric results

Figure 2a includes model predicted zonal-mean temperatures for the winter months at 80°N as well. The heavy, solid curve is the simulation of the present climate using CAM3; it attempts to replicate the observational data (dotted). Note that there is a cold bias in the lower stratosphere of the model, which has occurred in all versions of CAM in this region of the atmosphere. The curves from the two simulations with

a weak surface temperature gradient are plotted as well; all three simulations keep average temperatures above the frost point. The coldest temperatures occur in the simulation RAD in which high loads of carbon dioxide cause a substantial longwave cooling to space in the middle and upper stratosphere. At these low pressures, however, temperatures would have to be colder still before reaching the frost point. WTG, which has a weaker surface temperature gradient but is otherwise identical to Present, shows little departure from the simulation of the present climate.

The dark gray area on the left side of the plot represents those temperatures and pressures at which a parcel of air containing 5 ppmv water vapor will be saturated. If methane were higher in warm climates, there might be an increase in the stratospheric concentration of water vapor owing to this chemical source. Schmidt and Shindell (2003) examined this problem and found that a tenfold increase in methane would triple the stratospheric concentrations of water vapor.[10] Should this chemical source be combined with a rise in the temperature of the tropical tropopause, ambient water vapor concentrations in the winter stratosphere could be higher in warm climates. But a threefold increase in water vapor from methane oxidation (Schmidt and Shindell 2003) and a warming of 5 K at the cold trap in the equatorial lower stratosphere would increase ambient stratospheric water vapor concentrations only modestly. For reference, the expanded range of temperatures and pressures that would be saturated if water vapor concentrations rose to 20 ppmv in the winter stratosphere are highlighted in light gray in Fig. 2. Note that even a fourfold increase in water vapor concentrations is insufficient to bring the frost point up to average temperatures in the Northern Hemisphere winter stratosphere. Of course, ambient concentrations for the winter stratosphere from the deep geologic past are unknown, but we include these estimates for reference.

The most surprising aspect of these soundings is their similarity in spite of such a significant change in the surface gradient. Had dynamical warming of the polar vortex significantly decreased in the climates with a weak surface gradient, temperatures there would cool toward radiative equilibrium. In fact, mean temperatures in the lowermost polar stratosphere showed a

slight increase from the simulation of the present climate.

Simulated winter temperatures in the Antarctic, which are shown in Fig. 2b, also show little change as a result of a weaker surface temperature gradient. The predicted temperature for Present is again colder than observations, but the simulations with weak surface temperature gradients predict temperatures will not be colder below 20 hPa. The impact of longwave cooling to space is clearly evident in RAD at high altitudes, as temperatures in the upper stratosphere are substantially lower than in the two other simulations (with present-day concentrations of carbon dioxide).

A comparison of the two hemispheres offers a nice example of the role of dynamics in setting large-scale temperatures in the winter stratosphere. Observational studies suggest that the residual circulation in the Southern Hemisphere is weaker than in the Northern Hemisphere, most likely owing to the fact that there is less planetary-scale wave generation [landmasses and topographic features are biased to the north of the equator, and this strongly affects planetary-wave formation; e.g., see Held and Hoskins (1985)]. In light of this, it is not surprising that Antarctic stratospheric winter temperatures change so little with a different surface gradient; the dynamical heating of the Antarctic vortex is already comparatively small.

A central question arises from the model results shown in Fig. 2: why, in spite of such strong differences in surface forcing, do temperatures show so much similarity across the simulations? We first present a closer look at the temperature and zonal wind structure of these simulations and then investigate the wave activity and residual circulations. As we shall see, the changes in the thermal stratification of the troposphere are crucial to keeping temperatures in the stratosphere similar across these simulations.

a. Zonal wind field

Because the direction and strength of the zonal winds govern the vertical propagation of planetary-scale waves into the stratosphere (Charney and Drazin 1961), we now examine the zonally symmetric, seasonal-mean state of these winds in the stratosphere. Figure 3a shows the zonal-mean zonal wind averaged over the last five Decembers, Januaries, and Februaries between the surface and 1 hPa for the Present simulation. As in the real atmosphere, there are two stratospheric jets: one easterly in the summer hemisphere and the other westerly in the winter one (westerly winds are shaded in gray). Note that the strong westerly winds in the winter hemisphere form the wall to the Arctic vortex. Winds increase with altitude (thermal

---

[10] But this finding depends somewhat on the concentrations of the hydroxyl radical, OH, which combines with methane to produce water. No information about its concentrations from the deep geologic past is available, and Schmidt and Shindell (2003) assumed its concentrations were equal to preindustrial levels.
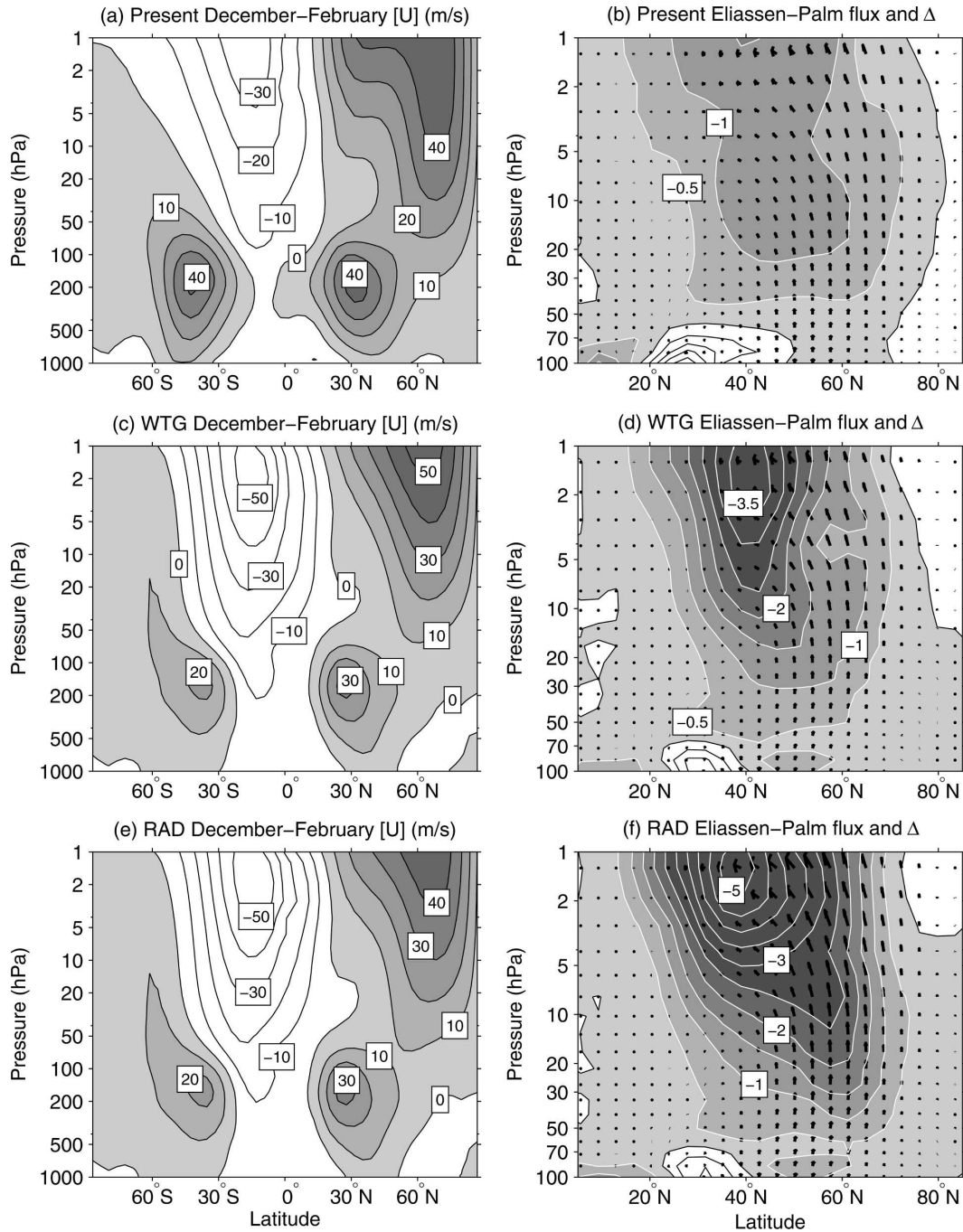
FIG. 3. (a) Zonal-mean zonal wind averaged over the last five Decembers, Januaries, and Februaries of Present; westerly winds are shaded. (b) $\widehat{\mathbf{F}}$ (arrows) and Δ (shaded contours) in the Northern Hemisphere stratosphere of Present; units of Δ are 10^{15} m³. As in (a), (b) but for (c), (d) WTG and (e), (f) RAD.

wind balance requires $\partial_z u \propto -\partial_y T$) and reach a maximum at the stratopause. The middle-latitude tropospheric jets are westerly in both hemispheres and reach a maximum amplitude at the tropopause, between 200 and 250 hPa.

The zonal-mean zonal winds for December–February from the WTG simulation are plotted in Fig. 3c. The stratospheric easterlies are stronger in WTG than in Present, but the stratospheric westerlies (shaded in gray) in the winter hemisphere are substantially weaker in the lower stratosphere. This is a critical point because the strength of the westerly jet determines what wave-

numbers can propagate into the stratosphere (Charney and Drazin 1961). The meridional temperature gradient in middle and high latitudes of the winter hemisphere at 100 hPa is less steep in WTG, primarily owing to a substantial increase in Arctic temperatures at this level. In section 5, we shall present some evidence that this warming results from a rise in the height of the extratropical tropopause in middle and high latitudes, thus lessening the planetary gradient of tropopause height and causing winds in the lower stratosphere to weaken in thermal wind balance.

WTG temperatures (not shown) in balance with this wind field are similar to those in Present through much of the stratosphere, but near and just above the tropical tropopause they are 2–6 K warmer in the WTG simulation than in Present. While Kirk-Davidoff et al. (2002) expected such a change owing to a weaker residual circulation (and less dynamical cooling of the tropical stratosphere), such a mechanism should also cool the middle- and high-latitude stratosphere, where the residual circulation downwells. There is no change in middle-latitude stratospheric temperatures, and they are several degrees warmer in the lower stratosphere.

The tropical tropopause warming may be caused by another mechanism here. While tropical surface temperatures do not change much between WTG and Present, they are nearly 30°C in the WTG simulation and are nearer to 27°C in the zonal mean in the Present (see Fig. 1). If the temperature profile in the tropical stratosphere is fixed by radiation (aside from water vapor, the concentrations of important radiative gasses are the same between these two simulations), then the surface temperature and tropospheric lapse rate determine the height and temperature of the tropopause (Held 1982; Thuburn and Craig 1997; Schneider 2004). Convection in the Tropics confines the tropospheric lapse rate to closely follow a moist adiabat; this keeps the tropical troposphere neutral to moist convection (Xu and Emanuel 1989). The combination of a higher surface temperature and a lapse rate confined to a moist adiabat requires that the tropopause be higher in the Tropics, as the intersection with a fixed stratospheric profile will occur at a warmer and higher point. This is an oversimplification of what sets the height of the tropical tropopause, but it illustrates to first order that a small rise in upper-tropospheric temperatures follows directly from a warmer surface temperature in the Tropics.[11]

In the RAD simulation, temperatures (not shown)

are much colder throughout the bulk of the stratosphere. Temperatures near the stratopause are as much as 25–30 K cooler in RAD than in Present (or in WTG); this is owing to the radiative cooling from increased concentrations of carbon dioxide, methane, and water vapor at high altitudes. Stratospheric longwave cooling to space increases with higher concentrations of carbon dioxide (e.g., Hartmann 1994). Temperatures are again a couple degrees warmer than in Present in the tropical lower stratosphere and in the Arctic lower stratosphere, but a reduction in the strength of the residual circulation should cause a warming of the tropical stratosphere along with a cooling of the Arctic. This pattern was not observed here. The zonal-mean zonal winds from RAD are shown in Fig. 3e. Like WTG, the westerly jet is weaker through much of the stratosphere than in Present, and this has implications for what wavenumbers are able to propagate into the stratosphere.

b. Dynamics

To understand the physics behind the thermal state of the winter stratosphere, we now examine the dynamics that force the stratosphere in each of these simulations. The set of transformed Eulerian mean equations (Andrews and McIntyre 1976) contain a single term that represents the eddy forcing of the stratosphere:

$$\frac{1}{\rho}\boldsymbol{\nabla}\cdot\mathbf{F} = [v^*q^*], \tag{7}$$

where $\mathbf{F}$ is the Eliassen–Palm flux (Eliassen and Palm 1961), q is the potential vorticity, asterisks denote departures from a zonal average, and square brackets indicate a zonal average. To graph this data in the latitude–pressure (ϕ, p) plane, the procedures of Edmon et al. (1980) are followed. In place of $\boldsymbol{\nabla}\cdot\mathbf{F}$, the divergence weighted by the mass of an annular ring $d\phi\,dp$ is used. Thus, we calculate a modified version of $\mathbf{F}$, denoted by a caret ($\hat{\ }$), using pressure as the vertical coordinate on a sphere:

$$\hat{\mathbf{F}} = (\widehat{F_\phi}, \widehat{F_p}) = \frac{2\pi a^3 \cos^2\phi}{g}\left(-\frac{1}{a}[u^*v^*], \frac{f[v^*\theta^*]}{S}\right), \tag{8}$$

where ϕ is latitude, a is the radius of the earth, f is the Coriolis parameter, and S is $d\theta/dp$ (Edmon et al. 1980). The form of the divergence of $\mathbf{F}$ used for contouring is

$$\Delta = \frac{\partial \widehat{F_\phi}}{\partial \phi} + \frac{\partial \widehat{F_p}}{\partial p}. \tag{9}$$

Equations (8) and (9) were calculated for each simulation, using data from the last five Decembers, Januaries, and Februaries of each.

---

[11] The divergence of moist adiabats at lower pressures also means tropical temperature in the upper troposphere will warm by a larger magnitude than at the surface.

Figure 3b shows $\hat{\mathbf{F}}$ and Δ for Present. The arrows show an upward propagation of eddy activity in the middle latitudes of the winter hemisphere that turns poleward in the upper stratosphere. Here it converges (indicated by the negative, shaded contours), and $\nabla \cdot \mathbf{F}$ acts as a body force on the winter stratosphere. The waves deposit angular momentum, damping the jet and driving a flow poleward in the upper stratosphere, in balance with the Coriolis torque. This poleward flow is connected to vertical flow by mass continuity: the flow is upward in the Tropics and downward at high latitudes.

Figure 3d shows $\hat{\mathbf{F}}$ and Δ for the WTG simulation. The convergence of wave activity in the upper stratosphere is larger than in Present, which shows that the force driving the residual circulation has increased in intensity. Indeed, the flux of $\mathbf{F}$ across the 100-hPa surface is larger in this case than in the Present simulation. It is larger in the upper troposphere as well, becoming equal between 400 and 500 hPa. Below this level, $\mathbf{F}$ is larger in the Present case; we shall examine these structures more closely in section 4c.

One clear difference between the Present and WTG cases is the decrease in upper-tropospheric and lower-stratospheric zonal winds in the WTG experiment; this has consequences for the spectral range of waves vertically propagating to high altitudes. The amplitudes of the first six stationary waves have all decreased in the lower troposphere, particularly in some of the synoptic-scale waves (not shown); yet the vertical component of $\mathbf{F}$ increases at all pressure levels above 400 hPa. This indicates that, although wave activity in the lower troposphere has decreased on the whole, the fraction of wave activity that is propagating vertically into the upper troposphere and lower stratosphere has increased. Rind et al. (1990) found a similar result in a middle atmosphere model forced with higher concentrations of carbon dioxide and a sea surface temperature gradient slightly weaker than that of our present climate.

In the RAD simulation, which contains both a weak temperature gradient and large concentrations of carbon dioxide and methane, the Eliassen–Palm flux is stronger still. Figure 3f shows the large convergence of wave activity in the middle and upper winter stratosphere. As in the WTG case, the flux of $\mathbf{F}$ across all pressure surfaces above 400 hPa increases in the winter hemisphere, even though the tropospheric energy decreases slightly.

Figure 4 shows the amplitude of the three longest stationary waves in the stratosphere (these were calculated from a time mean of the last five Decembers, Januaries, and Februaries). The amplitudes are greatest for the longest waves, in agreement with the predictions of Charney and Drazin (1961). In Present (Figs. 4a,c,e), there is a strong presence of the two longest planetary waves, but wavenumber 3 is evanescent. Observations of the winter stratosphere (e.g., Andrews et al. 1987) are quite similar, with wavenumber 3 and shorter waves absent. These shorter waves are largely prohibited from vertically propagating into the stratosphere by the strong winds in the tropospheric jet; the winds in the lower stratosphere are also too strong to allow for propagation of these short waves.

The amplitudes of the first three stationary waves for the boreal winter of the RAD simulation are shown in Figs. 4b, 4d, and 4f. (The amplitudes from WTG are quite similar to RAD, albeit with a smaller amplitude of wavenumber 1.) Compared to Present, there is little change in the amplitude of wavenumber 1, but there is an increase in the intensity of wavenumber 2. Wavenumber 3 has a closed maximum at stratospheric altitudes, whereas it was evanescent in the Present case. In both the WTG and RAD simulations, there is a new wave present in the winter stratosphere. This suggests that a shorter wave, which was absent in Present, is vertically propagating into the stratosphere in the WTG and RAD cases, contributing to the increased forcing by $\nabla \cdot \mathbf{F}$.

A few additional points are worth noting here. First, as seen in Fig. 5, the downwelling branch of the residual circulation is strongest in middle latitudes, especially in the Present simulation. This is especially true above 40 hPa where the circulation is actually closing off aloft; this difficulty has been observed in other models of the middle atmosphere, as the flow closes in the arbitrary frictional layer at the model top rather than at the ground (Semeniuk and Shepherd 2001). The simulated winter polar stratosphere has long been too cold in middle atmosphere models, and it is possible that poor resolution of the residual circulation is partially responsible, given the maturity of current radiative codes.

Second, some of the streamlines that do reach the lower stratosphere in the highest latitudes must have traveled above 2 hPa, a region in which the Rayleigh friction was imposed. To see how large an influence the amplitude of the Rayleigh friction can have on these results, we repeated the RAD experiment but cut the amplitude of the Rayleigh friction by a factor of 2. Temperatures were less than 1°C different up to 40 hPa and within 4°C up to 15 hPa. The jet speeds differed by less than 2 m s^{-1} below 15 hPa, while the maximum near the stratopause increased 10–15 m s^{-1} when the Rayleigh friction was reduced. While the effect on the temperatures in the lower and middle polar stratosphere appears small, this does underscore that gravity wave breaking in the mesosphere has an impact on tempera-
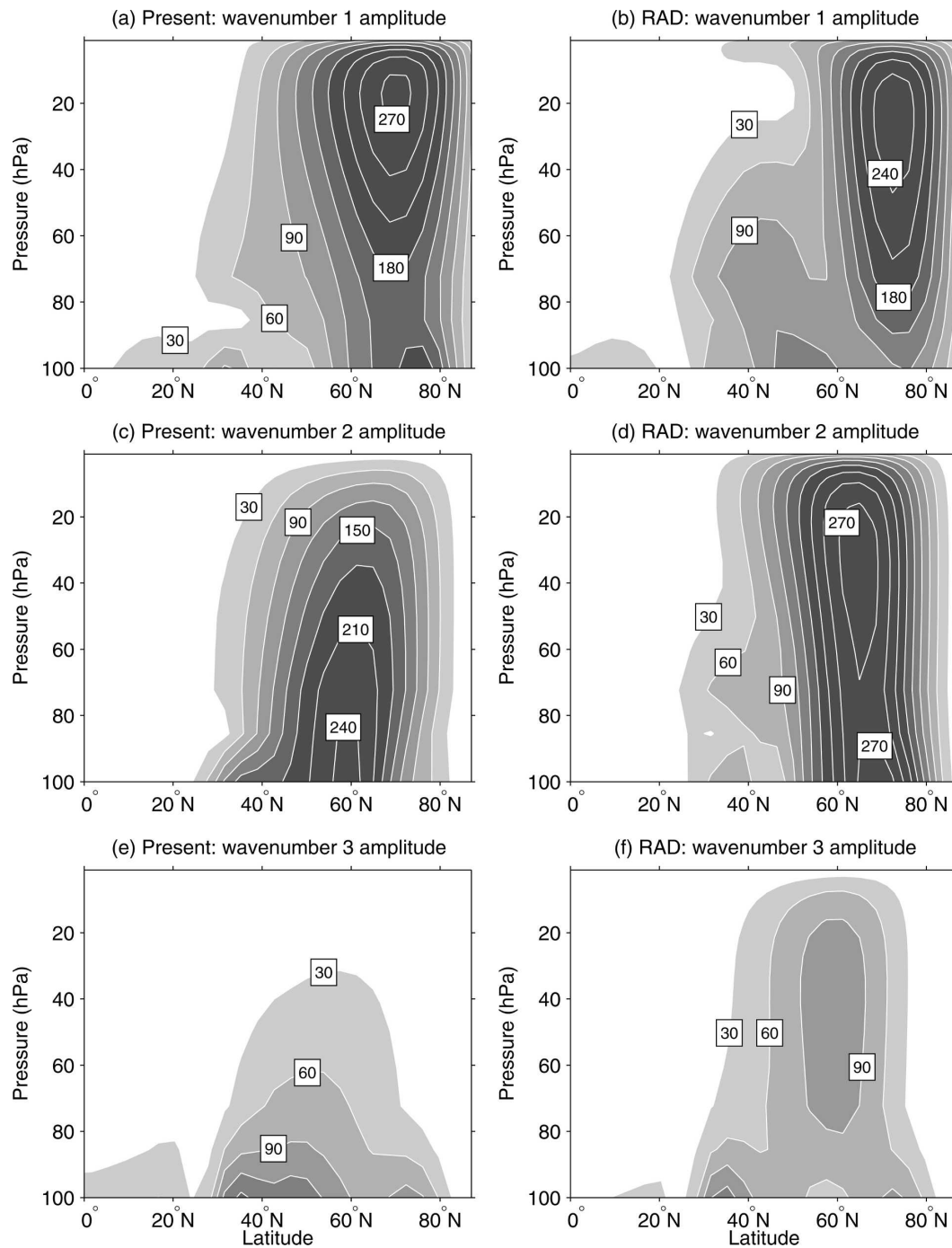
(a) Present: wavenumber 1 amplitude

(b) RAD: wavenumber 1 amplitude

(c) Present: wavenumber 2 amplitude

(d) RAD: wavenumber 2 amplitude

(e) Present: wavenumber 3 amplitude

(f) RAD: wavenumber 3 amplitude

FIG. 4. Amplitude of wavenumber 1 (normalized by $\sqrt{p/p_o}$ to compensate for increasing amplitudes with decreasing density) in (a) Present and (b) RAD computed from data averaged over the last five Decembers, Januaries, and Februaries; units are in m. As in (a), (b) but for (c), (d) wavenumber 2 and (e), (f) wavenumber 3.

tures in the polar vortex, and changes to surface topography and the stratification and mean wind structure of the middle atmosphere may yet influence how the polar stratosphere evolved at particular periods during the geologic past.

Because the intensity of the residual circulation increased in both of the simulations with a weak surface temperature gradient, the temperatures in the middle- and high-latitude stratosphere did not cool toward their radiative equilibrium values. Indeed the remarkable
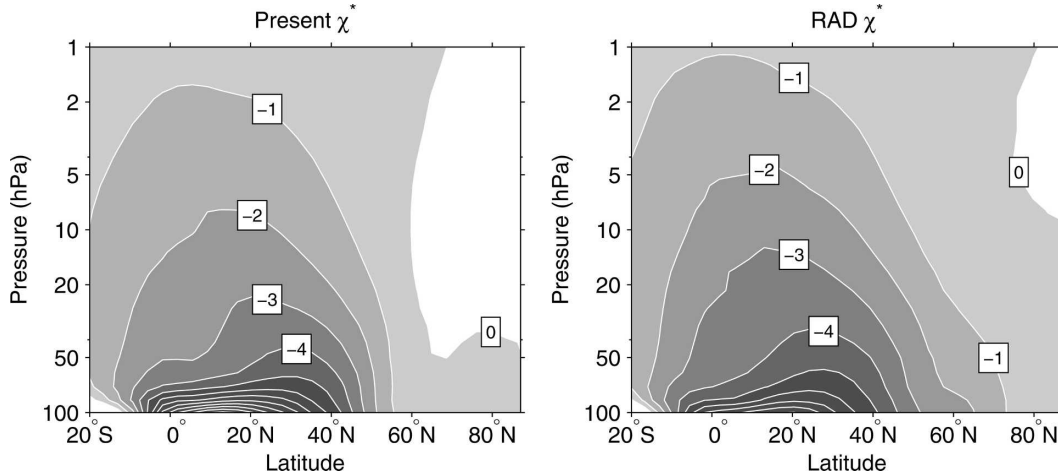
FIG. 5. The residual mean circulation in the stratosphere for (a) Present and (b) RAD. The flow circulates clockwise around negative contours. Contours are plotted and labeled every 10^9 kg s^{-1}.

similarity in the zonal-mean time-mean soundings shown in Fig. 2 seems consistent with the intensity of the dynamic forcing. In the next section, we examine the propagation of these waves through the troposphere and consider the energy characteristics of the simulations.

c. Wave propagation and energy

We calculated a complete energy budget for the full atmosphere and, separately, for the stratosphere (bounded below by the 100-hPa surface). The kinetic and potential energies in the mean flow, transient eddies, and stationary eddies decreased substantially in the simulations with a weak temperature gradient; the decrease was most precipitous in the troposphere and in the mean flow and transient eddies. This was true of the annual averages as well as the seasonal extremes, which Rind et al. (1990, 1998) also reported. The stratosphere has a much smaller amount of energy, but it also occupies only 10% of the atmospheric mass. Unlike the full atmosphere, there is no period during which conversion from available potential energy to kinetic energy can offset frictional dissipation (Dopplick 1971). Boundary terms on the 100-hPa pressure surface, which we take to be the lower bound of the stratosphere, account for the transfer of energy from the troposphere below to the stratosphere above. The boundary terms dominate the energy budget of the stratosphere: rather than being internally generated, energy is transported from the lower atmosphere (Charney and Drazin 1961; Charney and Pedlosky 1963; Oort 1964; Muench 1965; Dopplick 1971).

While the energetics of the full atmosphere decrease by a sizable fraction in the WTG and RAD simulations, the decrease in the stratosphere is comparatively small. Most forms of energy decrease above 100 hPa, but the kinetic and available potential stationary eddy energy actually grow. While the entire atmosphere has become less energetic, the stratosphere has decreased by a much smaller fraction. The stratosphere is selective in what it accepts from the troposphere; only the longest planetary waves are able to propagate vertically (Charney and Drazin 1961). The addition of wavenumber 3, illustrated in Fig. 4f, coupled with the similar amplitude of wavenumbers 1 and 2, has kept the energy of the stratosphere high and the residual circulation strong.

Energy is not Galilean invariant, of course, and this can lead to a misleading picture. What matters for the stratosphere is the wave activity admitted from the troposphere, which will ultimately drive the residual circulation by breaking and depositing angular momentum in the upper stratosphere. The decreases in energy say nothing about the wave propagation. The boundary terms at the 100-hPa surface continue to dominate the energy cycle of the stratosphere in the warm climate runs, although they too have decreased from Present. This is a consequence of the decrease in the zonal mean wind. Eliassen and Palm (1961) showed that the upward flux of wave energy is equal to the product of the vertical component of the Eliassen–Palm flux and the zonal wind. As we shall see below, the vertical component of the Eliassen–Palm flux across 100 hPa increases in the warm climates, but the zonal-mean zonal wind dropped by about a factor of 2 (see Figs. 3c,e); thus, the decrease in the boundary energy terms does not reflect a change in wave activity.
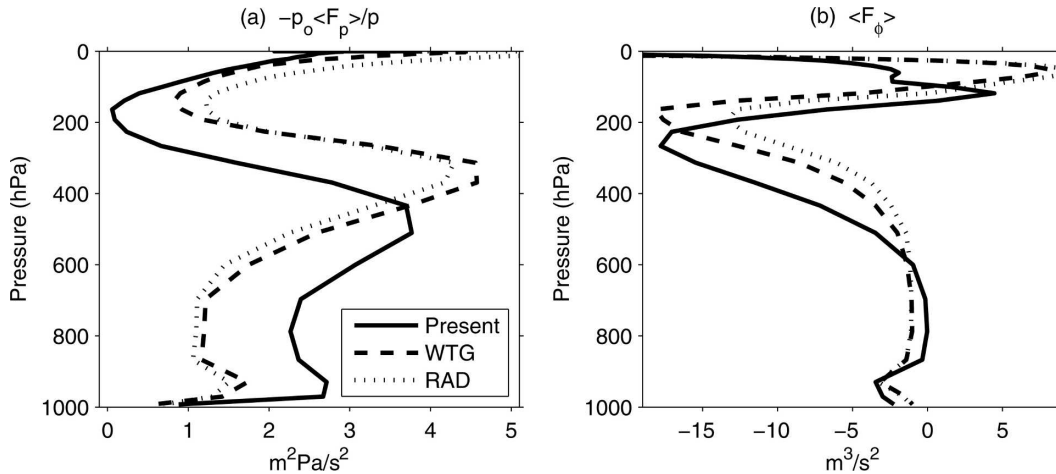
FIG. 6. Isobaric mean values of (a) the vertical component of **F** (normalized by $-p_o/p$) and (b) the horizontal component over the Northern Hemisphere polar cap bounded by 30°N. Positive values in (a) indicate an upward flux.

In Fig. 6, the isobaric mean values of the vertical and horizontal components of the extratropical Northern Hemisphere Eliassen–Palm flux **F** are shown for the three simulations. These averages, denoted by angle brackets, were calculated on each pressure surface over a polar cap bounded by 30°N. Note that the vertical component F_p (Fig. 6a) has been multiplied by -1 so that positive values correspond to an upward flux (toward decreasing pressure). The vertical component was also normalized by p_o/p in order to retain resolution at higher altitudes in the figure.

The vertical component, which is proportional to the eddy flux of heat, is larger in the lower troposphere in the Present simulation than in the two warmer climate ones. This is consistent with stronger eddies and more generation in the present climate and a decrease in eddy energy during warm climates. By the middle troposphere, however, **F** acquires an equatorward tilt in the Present simulation as the strong tropospheric jet deflects eddy energy equatorward. In contrast, the vertical component of **F** in the warm climate states remains strong through the upper troposphere. This suggests that the weaker tropospheric jet in the warm climates, which is in balance with a weak meridional temperature gradient, permits more eddies to pass into the lower stratosphere in spite of the fact that fewer are generated in the lower troposphere.[12] This is consistent with the strong forcing of the residual mean circulation presented in the previous section.

5. Tropospheric thermal stratification

Underlying the similarities of the stratospheric structure and dynamics are rather interesting changes in the stratification of the troposphere. The weak temperature gradient imposed at the surface has also forced weak gradients throughout the depth of the troposphere, which are responsible for the decrease in the zonal winds. There is some indication that the physics governing extratropical stratification is different between WTG and RAD and Present. Soundings from three model points are shown in Fig. 7;[13] these data were averaged over the last five Decembers, Januaries, and Februaries from Present (Fig. 7a) and RAD (Fig. 7b). The dotted curves are moist adiabats, which have constant values of saturation equivalent potential temperature θ_e^* (Emanuel 1994). As representative of soundings from the Tropics, note that the sounding from Hawaii in Present features tropospheric temperatures confined to a moist adiabat throughout the depth of the troposphere, underscoring the importance of moist convection to setting the thermal stratification at these latitudes (Xu and Emanuel 1989). This physics appears unaltered in the simulations featuring weak temperature gradients.

By contrast, soundings from middle and high latitudes feature vertical profiles decidedly stable to vertical moist convection in the present climate (Stone and

---

[12] Note also that **F** acquires an equatorward tilt at a higher altitude in the upper troposphere of the warm climate states, consistent with a higher jet and extratropical tropopause.

---

[13] The actual model point for Hawaii is located at 20.4°N, 157.5°W; the actual model point in central North America is at 46.4°N, 101.2°W, which is in present-day North Dakota. The sounding from the North Pole was computed by taking a zonal average around 87.2°N, the northernmost latitude in the model.
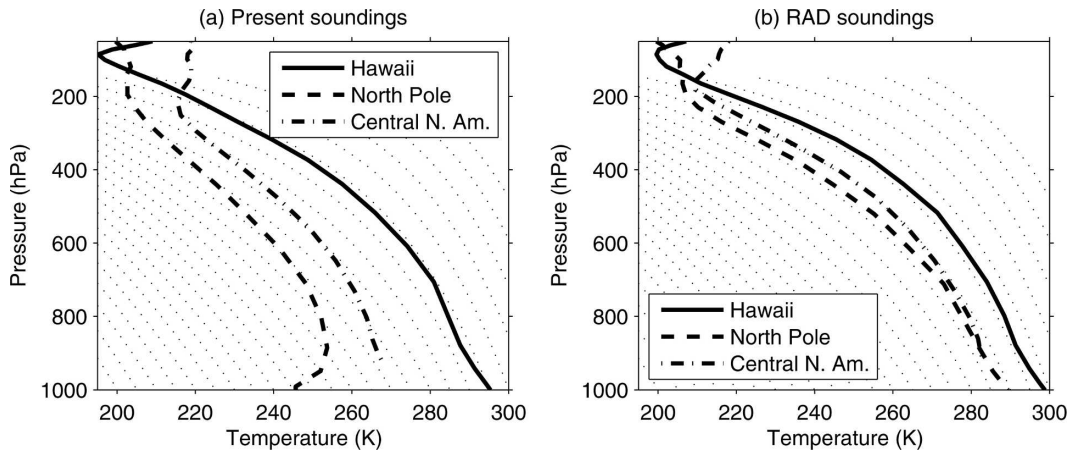
FIG. 7. Modeled December–February soundings from a point in the Tropics (solid), the North Pole (dashed), and the North American Great Plains (dashed–dotted) from (a) Present and (b) RAD. The dotted curves are moist adiabats.

Carlson 1979; Schneider 2007), and the model-predicted soundings at the North Pole and over the North American continent are consistent with these observations. The sounding from the North Pole in Present (Fig. 7a) features a low-level inversion, which is a common feature of winter Arctic soundings. One of the most interesting features of the simulations forced with a weak surface temperature gradient is that the vertical soundings at these latitudes become confined to a moist adiabat all the way to the poles. As seen in Fig. 7b, this is true over the continents as well, where temperatures were not specified explicitly, and remains true through all seasons. (This is true of WTG, too.) This suggests that, as the eddies have weakened, convection establishes the extratropical thermal stratification. Schneider and Walker (2006) have found a similar transition in a simplified general circulation model. Huber and Sloan (1999) also found that deep convection increased at high latitudes in simulations of the LPTM.

It appears that convection is dominating the tropospheric stratification at all latitudes and in all seasons in these warm climate simulations. To some extent, this is not surprising as the eddies are weak and the imposed surface temperatures are warm and convectively unstable. But the nearly ubiquitous convective adjustment raises an interesting question: could moist convection or slantwise moist convection set the tropospheric stratification during warm climates? If so, the consequences for the atmospheric heat flux are interesting. Though it is hard to imagine that convection itself could ever control the meridional heat flux, it could strongly affect the eddies that do so through its control on the tropospheric stratification.

6. Conclusions

Our results suggest that a dynamic feedback between the surface climate and the winter stratosphere may be complicated by changes in tropopause height, tropospheric thermal stratification, and concomitant changes in the zonal wind field. Of course the stratosphere during a particular time period (such as Paleocene or Eocene epochs) may have differed significantly from the simulations that we presented here because of changes to topography, continental location, the chemical composition of the atmosphere, or some combination of factors; our purpose was merely to investigate how easily the stratosphere might reach a state more conducive to the formation of polar stratospheric clouds in response to a weakening of the surface temperature gradient alone. The physics controlling stratification may produce a significant obstacle.

We have found that winter stratospheric temperatures do not change significantly when the surface temperature gradient is greatly weakened. This surprising result comes from an increase in the vertical component of the Eliassen–Palm flux in the upper troposphere and lower stratosphere as the westerly jets weaken. The vertical flux of wave activity increases in spite of the fact that the generation of eddies in the lower atmosphere decreases when the surface temperature gradient weakens. The vertical flux of wave activity dampens the stratospheric jet, forces a strong residual circulation, and holds winter stratospheric temperatures nearly constant across these simulations. This robust vertical propagation is made possible because the weak temperature gradient imposed at the surface forced a weaker meridional gradient throughout the full depth
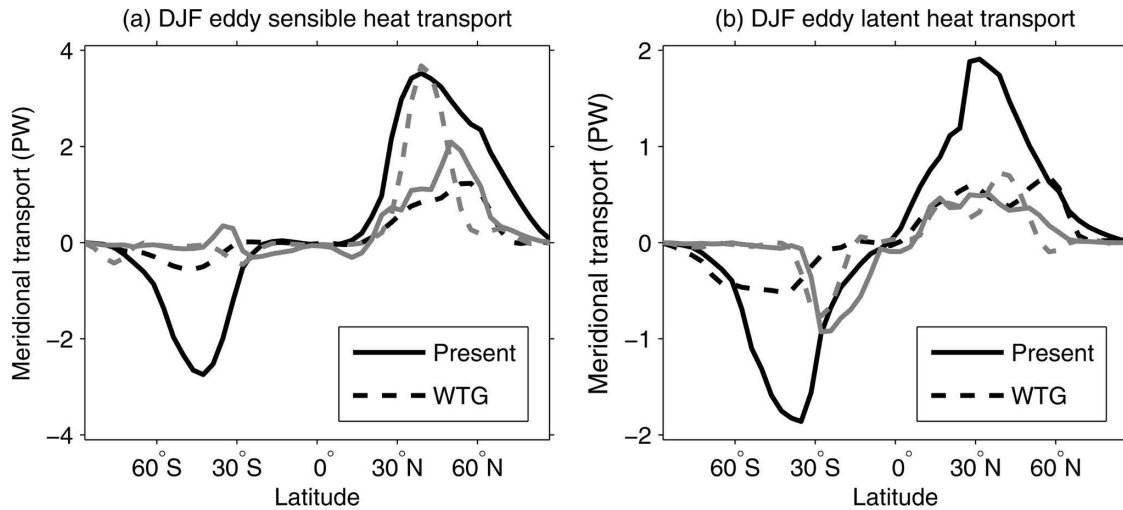
FIG. 8. The transport of (a) sensible heat and (b) latent heat by transient (black) and stationary (gray) eddies in December–February in Present (solid) and WTG (dashed).

of the troposphere, which requires a concomitant weakening of the westerly jets in thermal wind balance. Winds in the lower stratosphere also weaken in the winter hemisphere, which allowed for the vertical propagation of wavenumber 3.

If the thermal stratification is maintained by convection at all latitudes during warm climates with weak surface temperature gradients, the balanced zonal wind field will be weaker than today. Our results should therefore be reproducible in other general circulation models whenever a transition to a convectively controlled extratropical thermal stratification occurs. Schneider and Walker (2006) have found such a transition in an idealized general circulation model when surface temperature gradients and eddy activity weaken.

While our results indicate that changes in the surface temperature gradient alone may be insufficient to alter winter stratospheric temperatures, specific time periods may have offered other routes to a colder polar stratosphere. The stratospheric residual circulation weakened in the Paleocene study conducted by Rind et al. (2001), and our findings suggest that the reduced topography and altered continental locations, rather than the weak SST gradient, were likely important factors in producing this behavior. A thorough investigation of changes in the generation of planetary-scale wave activity owing to the reduced topography of the Eocene and Paleocene epochs is beyond the scope of our paper, but some insight can be gained by comparing the two hemispheres in Fig. 2. The Southern Hemisphere today has far less land and topography than does the Northern Hemisphere, and temperatures are colder in the

Antarctic polar vortex than in the Arctic one. As a result, the overturning circulation is weaker and temperatures are colder in the Southern Hemisphere winter. Still, observational studies of polar stratospheric clouds (Rosenfield 1992, 1993) show that such clouds have little impact on surface temperatures today, and thicker clouds would require a large increase in stratospheric water vapor concentrations, which in turn would increase absorption of longwave radiation and affect temperatures in their environment. Further study is required to assess whether optically thick clouds are thermodynamically viable in the stratosphere.

The early Cenozoic climates still pose the question of how the atmosphere could sustain a flux of enthalpy to the highest latitudes in the presence of a weak surface temperature gradient. We show the December–February average eddy heat transports of sensible and latent heat in Fig. 8. The WTG simulation has a sizable reduction in the transport of sensible heat by transient eddies; transport by stationary eddies has not diminished in WTG, which is consistent with the constancy of the stratospheric forcing observed earlier in the paper. Transport of latent heat by transient eddies has diminished substantially in the presence of a weakened temperature gradient. Caballero and Langen (2005) found that the latent heat flux was dependent on the strength of the surface temperature gradient (and largely independent of the mean temperature) during warm climates in an idealized general circulation model. Pierrehumbert (2002) found that, while the latent heat flux grew in a coupled simulation of the Eocene, which produced hot tropical temperatures, its magnitude was insufficient to strongly affect the temperature gradient. It

is intriguing to wonder if there is an optimal meridional entropy gradient at which the latent heat flux reaches a maximum value.

Other proposals include a climate state with an equator-to-pole Hadley cell (Farrell 1990). Such a state might be maintained if momentum transport by convection were strong enough to generate sufficient frictional dissipation to overcome angular momentum conservation in the upper troposphere, but tests of this idea may depend on the details of model convective parameterizations. With warmer estimates of Eocene tropical temperatures (e.g., Pearson et al. 2001), early ideas regarding high loads of carbon dioxide (e.g., Barron and Washington 1985) and other greenhouse gases are likely a central part of the problem. Enhanced mixing in the upper tropical oceans by tropical cyclones might have provided a cooling mechanism in the Tropics (Korty et al. 2007).

REFERENCES

Andrews, D. G., and M. E. McIntyre, 1976: Planetary waves in horizontal and vertical shear: The generalized Eliassen–Palm relation and the mean zonal acceleration. *J. Atmos. Sci.,* **33,** 2031–2048.

——, J. R. Holton, and C. B. Leovy, 1987: *Middle Atmosphere Dynamics.* Academic Press, 489 pp.

Barron, E. J., 1983: A warm, equable Cretaceous: The nature of the problem. *Earth-Sci. Rev.,* **19,** 305–338.

——, and W. M. Washington, 1985: Warm Cretaceous climates: High atmospheric CO_2 as a plausible mechanism. *The Carbon Cycle and Atmospheric CO_2: Natural Variations Archean to Present, Geophys. Monogr.,* Vol. 32, Amer. Geophys. Union, 546–553.

Boville, B. A., 1986: Wave–mean flow interactions in a general circulation model of the troposphere and stratosphere. *J. Atmos. Sci.,* **43,** 1711–1725.

Bralower, T., D. J. Thomas, J. C. Zachos, M. M. Hirschmann, U. Röhl, H. Sigurdsson, E. Thomas, and D. L. Whitney, 1997: High-resolution records of the late Paleocene thermal maximum and circum-Caribbean volcanism: Is there a causal link? *Geology,* **25,** 963–966.

Caballero, R., and P. L. Langen, 2005: The dynamic range of poleward energy transport in an atmospheric general circulation model. *Geophys. Res. Lett.,* **32,** L02705, doi:10.1029/2004GL021581.

Carslaw, K. S., B. P. Luo, S. L. Clegg, T. Peter, P. Brimblecombe, and P. J. Crutzen, 1994: Stratospheric aerosol growth and

HNO_3 gas phase depletion from coupled HNO_3 and water uptake by liquid particles. *Geophys. Res. Lett.,* **21,** 2479–2482.

Charney, J. G., and P. G. Drazin, 1961: Propagation of planetary-scale disturbances from the lower into the upper atmosphere. *J. Geophys. Res.,* **66,** 83–109.

——, and J. Pedlosky, 1963: On the trapping of unstable planetary waves in the atmosphere. *J. Geophys. Res.,* **68,** 6441–6442.

Collins, W. D., and Coauthors, 2006: The formulation and atmospheric simulation of the Community Atmosphere Model version 3 (CAM3). *J. Climate,* **19,** 2144–2161.

Dickens, G., M. M. Castillo, and J. C. G. Walker, 1997: A blast of gas in the latest Paleocene: Simulating first-order effects of massive dissociation of oceanic methane hydrate. *Geology,* **25,** 259–262.

Dickinson, R. E., K. W. Oleson, G. Bonan, F. Hoffman, P. Thornton, M. Vertenstein, Z.-L. Yang, and X. Zeng, 2006: The Community Land Model and its climate statistics as a component of the Community Climate System Model. *J. Climate,* **19,** 2302–2324.

Dopplick, T. G., 1971: The energetics of the lower stratosphere including radiative effects. *Quart. J. Roy. Meteor. Soc.,* **97,** 209–237.

Edmon, H. J., Jr., B. J. Hoskins, and M. E. McIntyre, 1980: Eliassen–Palm cross sections for the troposphere. *J. Atmos. Sci.,* **37,** 2600–2616.

Eliassen, A., and E. Palm, 1961: On the transfer of energy in stationary mountain waves. *Geofys. Publ.,* **22,** 1–23.

Emanuel, K. A., 1994: *Atmospheric Convection.* Oxford University Press, 580 pp.

——, 2002: A simple model of multiple climate regimes. *J. Geophys. Res.,* **107,** 4077, doi:10.1029/2001JD001002.

Farrell, B. F., 1990: Equable climate dynamics. *J. Atmos. Sci.,* **47,** 2986–2995.

Hartmann, D. L., 1994: *Global Physical Climatology.* Academic Press, 411 pp.

Held, I. M., 1982: On the height of the tropopause and the static stability of the troposphere. *J. Atmos. Sci.,* **39,** 412–417.

——, and B. J. Hoskins, 1985: Large-scale eddies and the general circulation of the troposphere. *Advances in Geophysics,* Vol. 28, Academic Press, 3–31.

Huber, B. T., K. G. Macleod, and S. L. Wing, Eds., 2000: *Warm Climates in Earth History.* Cambridge University Press, 462 pp.

Huber, M., and L. C. Sloan, 1999: Warm climate transitions: A general circulation modeling study of the Late Paleocene Thermal Maximum (~56 Ma). *J. Geophys. Res.,* **104,** 16 633–16 655.

——, and ——, 2000: Climatic responses to tropical sea surface temperature changes on a "greenhouse" Earth. *Paleoceanography,* **15,** 443–450.

Kent, G. S., L. R. Poole, and M. P. McCormick, 1986: Characteristics of Arctic polar stratospheric clouds as measured by airborne lidar. *J. Atmos. Sci.,* **43,** 2149–2161.

Kirk-Davidoff, D. B., D. P. Schrag, and J. G. Anderson, 2002: On the feedback of stratospheric clouds on polar climate. *Geophys. Res. Lett.,* **29,** 1556, doi:10.1029/2002GL014659.

Korty, R. L., K. A. Emanuel, and J. R. Scott, 2007: Tropical cyclone–induced upper-ocean mixing and climate: Application to equable climates. *J. Climate,* in press.

Lindzen, R. S., 1990: *Dynamics in Atmospheric Physics: Lecture Notes for an Introductory Graduate-Level Course.* Cambridge University Press, 310 pp.

——, and B. Farrell, 1980: The role of polar regions in global

climate, and a new parameterization of global heat transport. *Mon. Wea. Rev.,* **108,** 2064–2079.

MacKenzie, A. R., M. Kulmala, A. Laaksonen, and T. Vesala, 1995: On the theories of type 1 polar stratospheric cloud formation. *J. Geophys. Res.,* **100,** 11 275–11 288.

Moran, K., and Coauthors, 2006: The Cenozoic palaeoenvironment of the Arctic Ocean. *Nature,* **441,** 601–605.

Muench, H. S., 1965: On the dynamics of the wintertime stratosphere circulation. *J. Atmos. Sci.,* **22,** 349–360.

O'Connell, S., M. A. Chandler, and R. Ruedy, 1996: Implications for the creation of warm saline deep water: Late Paleocene reconstructions and global climate model simulations. *Geol. Soc. Amer. Bull.,* **100,** 270–284.

Oort, A. H., 1964: On the energetics of the mean and eddy circulations in the lower stratosphere. *Tellus,* **16,** 309–327.

Pearson, P. N., P. W. Ditchfield, J. Singano, K. G. Harcourt-Brown, C. J. Nicholas, R. K. Olsson, N. J. Shackleton, and M. A. Hall, 2001: Warm tropical sea surface temperatures in the Late Cretaceous and Eocene epochs. *Nature,* **413,** 481–487.

Peters, R. B., and L. C. Sloan, 2001: High concentrations of greenhouse gases and polar stratospheric clouds: A possible solution to high latitude faunal migration at the latest Paleocene thermal maximum. *Geology,* **28,** 979–982.

Pierrehumbert, R. T., 2002: The hydrologic cycle in deep-time climate problems. *Nature,* **419,** 191–198.

Rayner, N. A., D. E. Parker, E. B. Horton, C. K. Folland, L. V. Alexander, D. P. Powell, E. C. Kent, and A. Kaplan, 2003: Global analyses of sea surface temperature, sea ice, and night marine air temperature since the late nineteenth century. *J. Geophys. Res.,* **108,** 4407, doi:10.1029/2002JD002670.

Rees, D., J. J. Barnett, and K. Labitzke, Eds., 1990: *COSPAR International Reference Atmosphere Models: 1986. Part II: Middle Atmosphere Models.* Vol. 10. Pergamon Press, 520 pp.

Remsberg, E., J. M. Russell III, L. L. Gordley, J. C. Gille, and P. L. Baily, 1984: Implications of the stratospheric water vapor distribution as determined from the Nimbus 7 LIMS experiment. *J. Atmos. Sci.,* **41,** 2934–2945.

Reynolds, R. W., N. A. Rayner, T. M. Smith, D. C. Stokes, and W. Wang, 2002: An improved in situ and satellite SST analysis for climate. *J. Climate,* **15,** 1609–1625.

Rind, D., R. Suozzo, N. K. Balachandran, A. Lacis, and G. Russell, 1988a: The GISS global climate-middle atmosphere model. Part I: Model structure and climatology. *J. Atmos. Sci.,* **45,** 329–370.

——, ——, and ——, 1988b: The GISS global climate-middle atmosphere model. Part II: Model variability due to interactions between planetary waves, the mean circulation and gravity wave drag. *J. Atmos. Sci.,* **45,** 371–386.

——, ——, ——, and M. J. Prather, 1990: Climate change and the middle atmosphere. Part I: The doubled CO_2 climate. *J. Atmos. Sci.,* **47,** 475–494.

——, D. Shindell, P. Lonergan, and N. K. Balachandran, 1998: Climate change and the middle atmosphere. Part III: The doubled CO_2 climate revisited. *J. Climate,* **11,** 876–894.

——, M. Chandler, P. Lonergan, and J. Lerner, 2001: Climate change and the middle atmosphere; 5. Paleostratosphere in cold and warm climates. *J. Geophys. Res.,* **106,** 20 195–20 212.

Rosenfield, J. E., 1992: Radiative effects of polar stratospheric clouds during the Airborne Antarctic Ozone Experiment and the Airborne Arctic Stratospheric Expedition. *J. Geophys. Res.,* **97,** 7841–7858.

——, 1993: Radiative feedback of polar stratospheric clouds on Antarctic temperatures. *Geophys. Res. Lett.,* **20,** 1195–1198.

Schmidt, G. A., and D. T. Shindell, 2003: Atmospheric composition, radiative forcing, and climate change as a consequence of a massive methane release from gas hydrates. *Paleoceanography,* **18,** 1004, doi:10.1029/2002PA000757.

Schneider, T., 2004: The tropopause and the thermal stratification in the extratropics of a dry atmosphere. *J. Atmos. Sci.,* **61,** 1317–1340.

——, 2007: The thermal stratification of the extratropical troposphere. *The Global Circulation of the Atmosphere,* T. Schneider and A. H. Sobel, Eds., Princeton University Press, 47–77.

——, and C. C. Walker, 2006: Self-organization of atmospheric macroturbulence into critical states of weak nonlinear eddy–eddy interactions. *J. Atmos. Sci.,* **63,** 1569–1586.

Semeniuk, K., and T. G. Shepherd, 2001: The middle-atmosphere Hadley circulation and equatorial inertial adjustment. *J. Atmos. Sci.,* **58,** 3077–3096.

Sloan, L. C., and D. Pollard, 1998: Polar stratospheric clouds: A high latitude warming mechanism in an ancient greenhouse world. *Geophys. Res. Lett.,* **25,** 3517–3520.

——, J. C. G. Walker, T. C. Moore Jr., D. K. Rea, and J. C. Zachos, 1992: Possible methane-induced polar warming in the early Eocene. *Nature,* **357,** 320–322.

——, M. Huber, and A. Ewing, 1999: Polar stratospheric cloud forcing in a greenhouse world. *Reconstructing Ocean History: A Window into the Future,* F. Abrantes and A. C. Mix, Eds., Kluwer Academic, 273–293.

——, ——, T. J. Crowley, J. Sewall, and S. Baum, 2001: Effect of sea surface temperature configuration on model simulations of "equable" climate in the early Eocene. *Palaeogeogr. Palaeoclimatol. Palaeoecol.,* **167,** 321–335.

Sluijs, A., and Coauthors, 2006: Subtropical Arctic Ocean temperatures during the Palaeocene/Eocene thermal maximum. *Nature,* **441,** 610–613.

Smith, A. K., and L. V. Lyjak, 1985: An observational estimate of gravity wave drag from the momentum balance in the middle atmosphere. *J. Geophys. Res.,* **90,** 2233–2242.

Stone, P. H., 1978: Baroclinic adjustment. *J. Atmos. Sci.,* **35,** 561–571.

——, and J. H. Carlson, 1979: Atmospheric lapse rate regimes and their parameterization. *J. Atmos. Sci.,* **36,** 415–423.

Thompson, D. W. J., and S. Solomon, 2005: Recent stratospheric climate trends as evidenced in radiosonde data: Global structure and tropospheric linkages. *J. Climate,* **18,** 4785–4795.

Thuburn, J., and G. C. Craig, 1997: GCM tests of theories for the height of the tropopause. *J. Atmos. Sci.,* **54,** 869–882.

Xu, K.-M., and K. A. Emanuel, 1989: Is the tropical atmosphere conditionally unstable? *Mon. Wea. Rev.,* **117,** 1471–1479.